Physica E 182 (2026) 116571

Contents lists available at ScienceDirect

Physica E: Low-dimensional Systems and Nanostructures

journal homepage: www.elsevier.com/locate/physe

Transport efficiency and localization transitions in boundary-coupled Aubry–André quantum channels

D.G.P. da Silva [a], I.F.F. dos Santos [a], B.G.S. Souza [a], W.F. Magalhães [a,b], G.M.A. Almeida [a], F.A.B.F. de Moura [a,*]

[a] Instituto de Física, Universidade Federal de Alagoas – UFAL, Maceió, AL, Brazil
[b] Curso de Licenciatura em Matemática, Universidade Regional do Cariri, Campos Sales, 63150–000, Brazil

ARTICLE INFO

Editor: Rudolf Andreas Römer

Keywords:
Statistical mechanics
Anderson localization
Phase transitions
Aubry-André

ABSTRACT

We investigate the interplay between spatial localization and coherent quantum state transfer (QST) in finite one-dimensional Aubry-André chains within a source–channel–receiver architecture. While the metal–insulator transition at the critical potential strength $\lambda_c = 2$ formally separates extended from localized eigenstates, our numerical analysis reveals a significant degradation of transport efficiency well before this threshold. In the regime $1 \lesssim \lambda < 2$, we identify a dynamic transport crossover where the state transfer fidelity collapses despite the persistence of spatially extended eigenstates. By comparing the participation ratio with the Thouless energy, we demonstrate that this transport breakdown is not driven by wave-packet confinement, but is instead a consequence of spectral fragmentation and a strongly suppressed effective transport velocity. Furthermore, we evaluate the spectral correlation between boundary sites as a static diagnostic for transport robustness. Our results indicate that while the phase-averaged band-center mode ($E_0 = 0$) retains substantial spectral connectivity up to the vicinity of the critical point, slightly detuned states ($E_0 \neq 0$) undergo a rapid suppression of boundary correlations for $\lambda \gtrsim 1$. These findings highlight that spatial delocalization is a necessary but insufficient condition for high-fidelity communication in aperiodic channels. Consequently, we conclude that optimal QST in finite quasiperiodic systems is achieved deep within the extended regime ($\lambda \lesssim 1$), requiring weak system–lead coupling and near-resonant injection at the band center.

1. Introduction

Quantum state transfer (QST) represents a cornerstone capability in quantum information processing, enabling the coherent transmission of quantum states between spatially separated nodes without collapsing their delicate superposition properties [1,2]. Spin chains and other quasi-one-dimensional quantum systems have emerged as natural platforms for implementing quantum communication channels, offering scalable architectures for distributed quantum computation [3,4]. While perfect state transfer with unit fidelity has been theoretically achieved through precise engineering of coupling strengths in specific chain configurations [5,6], practical realizations face substantial obstacles from environmental decoherence, fabrication imperfections, and control limitations [7].

The introduction of aperiodic modulation in quantum chains has opened new paradigms for controlling quantum transport, revealing a regime between Anderson localization and ballistic propagation [8,9]. Aperiodic systems, characterized by long-range order without translational invariance, exhibit unique spectral properties that enable the engineering of quantum channels with tailored transport behavior [10,11]. The Aubry-André model provides an interesting example, displaying a localization-delocalization transition as the quasiperiodic potential strength is varied [8,12], offering precise control over wavefunction extent and propagation dynamics [13,14]. Recent studies have shown that properly designed aperiodic potentials can enhance quantum state transfer fidelity by isolating transport-mediating modes [15]. Deterministic sequences such as Fibonacci and Thue–Morse provide controllable aperiodicity that suppresses diffusion while preserving coherent transport [16,17]. Moreover, aperiodic modulation can improve robustness by breaking resonant symmetries and generating mobility edges [18], with related strategies explored in spin-chain quantum state transfer protocols [19]. Understanding how aperiodic potentials and their deformations influence transport is therefore crucial for designing robust quantum communication schemes in realistic environments [20,21].

In this work, we investigate quantum state transfer in a source–channel–receiver architecture using a modified Harper model, defined

* Corresponding author.
E-mail address: fidelis@fis.ufal.br (F.A.B.F. de Moura).

https://doi.org/10.1016/j.physe.2026.116571
Received 19 February 2026; Received in revised form 25 April 2026; Accepted 6 May 2026
Available online 13 May 2026

as the standard quasiperiodic Harper (Aubry–André) potential supplemented by an additional random global phase ϕ. This extension provides a controlled interpolation between deterministic quasiperiodicity and genuine disorder, allowing us to probe hybrid regimes relevant to realistic aperiodic quantum devices. The physical relevance of introducing disorder is well established in the literature [22]. While previous studies of the Aubry–André model have focused primarily on metal–insulator transitions and bulk localization properties, our approach highlights how the random phase reshapes dynamical subregimes within the delocalized phase when boundary couplings are explicitly taken into account. In particular, we demonstrate that ϕ acts as an effective disorder control parameter that modulates transport fidelity without destroying tunability, revealing optimal conditions for coherent state transfer that emerge from the interplay between intrinsic bulk structure and boundary-driven observables. By combining spatial participation ratios, spectral correlation measures, and time-dependent transfer fidelities, we uncover a hierarchy of transport efficiencies inside the delocalized regime, distinguishing genuinely ballistic dynamics from regimes dominated by spectral fragmentation. These results provide practical guidelines for designing robust aperiodic quantum interconnects operating in noisy, non-translationally invariant environments.

2. Physical model

We consider coherent quantum transport in a one-dimensional quasiperiodic lattice described by the Aubry-André model [23] with a random phase ϕ, coupled to an external source and an external receiver. The total Hamiltonian is $H = H_{\text{ch}} + H_{\text{sr}}$.

The channel Hamiltonian is given by:

$$H_{\text{ch}} = \sum_{n=1}^{N} \lambda \cos(2\pi\beta n + \phi) |n\rangle\langle n| + J \sum_{n=1}^{N-1} (|n\rangle\langle n+1| + |n+1\rangle\langle n|). \quad (1)$$

The source and receiver are coupled to the ends of the channel via:

$$H_{\text{sr}} = g(|s\rangle\langle 1| + |1\rangle\langle s|) + g(|N\rangle\langle r| + |r\rangle\langle N|) + E_0(|s\rangle\langle s| + |r\rangle\langle r|) \quad (2)$$

where g represents the coupling strength. To ensure the quasiperiodicity of the system and avoid commensurability effects, the parameter β must be an irrational number. In this study, we primarily adopt the golden ratio $\beta = (\sqrt{5}-1)/2$ as the standard modulation frequency. It is important to emphasize that our numerical investigations were extended to other irrational values as well as rational approximations of the golden ratio (i.e., the ratios of successive Fibonacci numbers F_{n-1}/F_n). In general, the results remained qualitatively consistent despite minor quantitative variations in some cases, confirming the robustness of the transport phenomena described herein. The phase ϕ is randomly chosen from the interval $[0, 2\pi]$. The dynamics are governed by the time evolution of an excitation initially at $|s\rangle$. In our calculations, the coupling g is generally smaller than the intra-channel coupling ($J = 1$).

To comprehensively characterize the system, we divide our analysis into two complementary frameworks. First, we examine the intrinsic localization properties of the isolated Aubry-André channel. Second, we investigate the efficiency of quantum state transfer within the full source–channel–receiver geometry. To evaluate the spectral and spatial properties of the channel without resorting to computationally expensive full diagonalization, we employ the retarded Green's function formalism. The specific elements are defined as [24,25]:

$$G_{ij}(E) = \langle i|(E - \hat{H}_{\text{ch}} + i\eta)^{-1}|j\rangle \quad (3)$$

where we adopt a numerical broadening $\eta = 10^{-3}$ J to ensure spectral convergence and handle the singularities of the propagator. By extracting the diagonal elements $G_{ii}(E)$, we obtain the Local Density of States (LDOS), $\rho_i(E) = -\frac{1}{\pi}\text{Im}[G_{ii}(E)]$, which reveals the density of available quantum states at specific lattice sites. To distinguish between extended and localized phases, we utilize the ratio $R(E) = \rho_{\text{geo}}/\rho_{\text{arith}}$ of the geometric to the arithmetic mean of the LDOS. This quantity acts as a useful statistical indicator, approaching unity in the metallic regime and becoming strongly suppressed in the localized regime as the distribution becomes log-normal. The statistical limits of the ratio $R(E)$ are fundamentally tied to the distribution of the LDOS across the lattice. In the metallic regime ($\lambda < 2$), the wavefunctions are delocalized and relatively uniform, which implies that the Local Density of States fluctuates minimally from site to site. In this case, the arithmetic and geometric means are comparable, and $R(E)$ approaches unity. As the system enters the localized phase ($\lambda > 2$), the LDOS becomes spatially sparse and follows a log-normal distribution, spanning several orders of magnitude. Consequently, the geometric mean, which is highly sensitive to the exponentially small values at sites far from the localization centers, drops significantly while the arithmetic mean remains finite, causing $R(E)$ to approach zero in the thermodynamic limit. It is worth noting, however, that for finite-sized systems and in the presence of numerical broadening, $R(E)$ does not vanish entirely, but rather saturates at a small residual value.

For the practical implementation of this formalism, we emphasize a high-performance numerical approach. To compute $G_{ij}(E)$, we avoid full matrix inversion, which typically scales as $\mathcal{O}(N^3)$, and instead reformulate the problem as a system of linear equations:

$$(E - \hat{H} + i\eta)\mathbf{g}_j = \mathbf{e}_j \quad (4)$$

where $\mathbf{g}_j$ represents the jth column of the Green's function matrix and $\mathbf{e}_j$ is the jth canonical basis vector. Given that the tight-binding Hamiltonian is restricted to nearest-neighbor hopping, the operator $(E - \hat{H} + i\eta)$ is tridiagonal. We exploit this sparsity by employing a specialized banded linear solver based on the Thomas algorithm. This reduces the computational complexity to $\mathcal{O}(N)$, allowing for the precise calculation of propagators and the density of states in large systems ($N \gg 10^3$) with minimal overhead. Furthermore, the spatial structure of the eigenstates is directly probed via the non-local propagator $G_{i,i+d}(E)$. The spatial decay of the wavefunctions is quantified by the spatial decay parameter $D(\lambda)$, which we numerically extract through an exponential fit of the average non-local propagator at the band center:

$$\langle|G_{1,1+d}(E=0)|\rangle \propto \exp(-Dd) \quad (5)$$

where the fit is performed over a wide range of distances d. A vanishing decay rate ($D \approx 0$) signifies extended wavefunctions, whereas a finite value ($D > 0$) confirms exponential confinement. Additionally, the neighbor propagator $\langle|G_{i,i+1}|\rangle$ provides a direct measure of local hybridization between adjacent sites. At the critical point $\lambda = 2$, the system undergoes a metal–insulator transition characterized by the closing of spectral gaps and the emergence of multifractal eigenstates. This critical resonance manifests as a pronounced peak in the neighbor propagator, identifying the regime of maximum susceptibility where the kinetic hopping J and the quasiperiodic potential λ are in exact competition. Physically, this peak arises from the crossover between two distinct suppression mechanisms: in the delocalized phase ($\lambda < 2$), the probability amplitude is diluted over the entire lattice ($1/N$ scaling), which naturally suppresses local correlations between any two specific sites; conversely, in the localized phase ($\lambda > 2$), exponential confinement drastically reduces the spatial overlap between neighbors due to the short localization length. Consequently, the critical point emerges as the locus of maximal local transmission amplitude, where the multifractal wavefunctions possess sufficient spatial extension to bridge adjacent sites without yet suffering the exponential penalty of the insulating regime.

Complementarily, we investigate the dynamical transport efficiency by calculating the Thouless energy $\mathcal{E}_T$ [26]. This is defined as the mean

energy shift of the spectrum when changing the boundary conditions of the isolated channel H_{ch} from periodic (PBC) to anti-periodic (APBC):

$$\mathcal{E}_T = \langle |\epsilon_k(\mathrm{PBC}) - \epsilon_k(\mathrm{APBC})| \rangle \tag{6}$$

In the delocalized phase, transport is characterized through the Thouless energy $\mathcal{E}_T$, obtained from the sensitivity of the spectrum to boundary conditions. From this energy scale, we define an effective transport velocity (Thouless velocity) as

$$\langle v_T \rangle \sim \frac{N\,\mathcal{E}_T}{\hbar}, \tag{7}$$

which follows from associating the Thouless time $\tau_T \sim \hbar/\mathcal{E}_T$ with the characteristic time required for an excitation to traverse a system of size N. Within this interpretation, the velocity can be expressed as $\langle v_T \rangle \sim L/\tau_T$, where $L \sim N$ represents the effective chain length in units of the lattice spacing. Thus, $\langle v_T \rangle$ provides a transport velocity scale derived from the spectral sensitivity. In our numerical calculations, we adopt units such that $J = 1$, $\hbar = 1$, and the lattice constant $a = 1$. Consequently, the Thouless velocity is expressed in natural units of $Ja/\hbar$. We emphasize that for $\lambda \to 0$, the extracted Thouless velocity approaches the clean-chain ballistic limit $v_T = 2Ja/\hbar$, validating the scaling relation. This diagnostic becomes particularly useful for revealing the dynamical transport crossover in the intermediate regime $1 \lesssim \lambda < 2$, where the eigenstates remain formally extended but transport becomes progressively hindered. In this regime, the quasiperiodic potential induces spectral fragmentation and band flattening, leading to a strong suppression of the Thouless velocity. As a result, transport slows down significantly despite the absence of full localization. For all results, we performed averaging over $M = 1000$ random realizations of the phase ϕ to ensure statistical convergence. The dynamical propagation is evaluated via the maximum fidelity $\bar{F}_{\max}$ within a time window $T_{\max} = 6 \times 10^5 \hbar/J$. This window is consistent with the perturbative estimate $T \sim 1/g^2$, ensuring that the complete evolution of the excitation is captured even when the transport speed is strongly reduced. The definition of $\langle v_T \rangle$ is valid within the delocalized regime ($\lambda < 2$), where the Thouless energy remains finite. In the localized phase ($\lambda > 2$), $\mathcal{E}_T$ decays exponentially with system size, and the corresponding Thouless velocity becomes exponentially suppressed, reflecting the breakdown of coherent transport.

Building upon these intrinsic bulk properties, we quantify the quantum state transfer efficiency and the nature of the eigenstates mediating the propagation. We begin with the Participation Ratio (PR), a spatial measure quantifying the number of lattice sites effectively occupied by an eigenstate. For an eigenmode $|\epsilon_k\rangle$ with components $V_{nk} = \langle n|\epsilon_k\rangle$, it is defined as $\mathrm{PR}_k = (\sum_{n=1}^{N} |V_{nk}|^4)^{-1}$, where values of PR $\sim N$ characterize extended states in the metallic phase ($\lambda < 2$), while PR $\sim \mathcal{O}(1)$ indicates exponential localization. Complementing this spatial perspective, we define the spectral weights $w_k^{(s)} = |V_{sk}|^2$ and $w_k^{(r)} = |V_{rk}|^2$ to measure the overlap of each mode k with the source (s) and receiver (r) sites, respectively. This enables the calculation of the static spectral correlation $C = \sum_k w_k^{(s)} w_k^{(r)}$, which serves as a measure of the channel's capacity to mediate transfer through the overlap of these weights. We emphasize that the spectral correlation is not proposed as a unique predictor, but as a complementary diagnostic correlated with transport properties . Finally, the dynamical propagation of an excitation initially localized at the source site $|s\rangle$ is governed by the amplitude $f(t) = \langle r|\, e^{-iHt}\, |s\rangle = \sum_k V_{rk} V_{sk}^* e^{-i\epsilon_k t}$. The transfer quality for an arbitrary qubit state is evaluated using the average fidelity $\bar{F}(t) = \frac{1}{2} + \frac{|f(t)|}{3} + \frac{|f(t)|^2}{6}$. The primary dynamical order parameter used to map the phase diagram is the maximum average fidelity achieved within a relevant time window $T_{\max}$, defined as $\bar{F}_{\max} = \max_{t\in[0,T_{\max}]} \bar{F}(t)$. For all disordered/quasiperiodic results presented, we performed averaging over $M = 1000$ random realizations of the phase ϕ to ensure statistical convergence (error bars are smaller than the symbol sizes). The maximum fidelity $\bar{F}_{\max}$ is searched within a time window $T_{\max} = 6\times10^5\ \hbar/\mathrm{J}$, which is sufficiently long to account for the velocity in the intermediate regime $1 < \lambda < 2$.

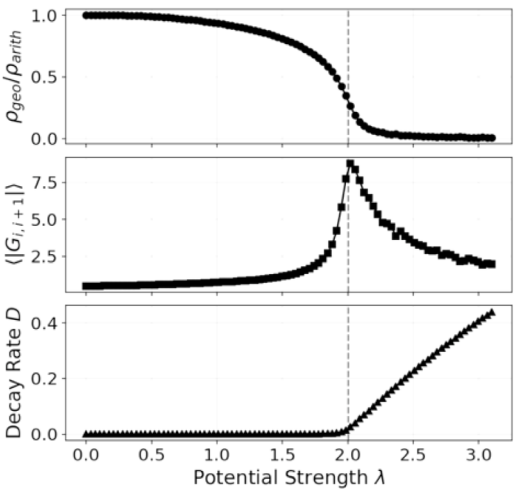

Fig. 1. Localization indicators derived from the retarded Green's function at the band center ($E = 0$). (Top) The LDOS ratio ρ_{geo}/ρ_{arith} marks the transition from extended to localized spectral statistics. (Middle) The neighbor propagator $\langle|G_{i,i+1}|\rangle$ peaks at $\lambda = 2$, reflecting critical state hybridization at the transition point. (Bottom) The spatial decay rate D remains null in the metallic phase and increases linearly for $\lambda > 2$, confirming the exponential localization of eigenstates.

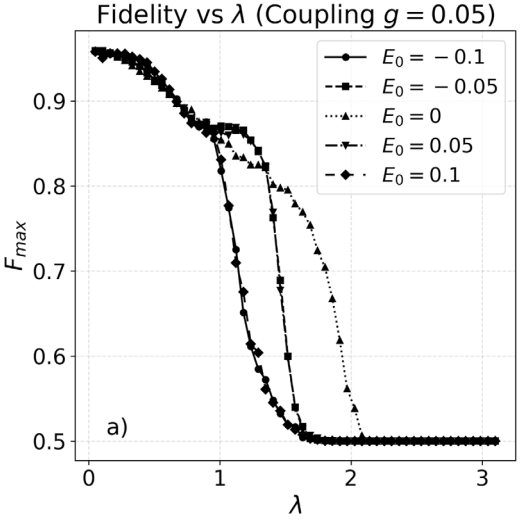

Fig. 2. Maximum fidelity (F_{max}) as a function of the parameter λ. High-efficiency transfer ($F_{max} \approx 1$) is restricted to the $\lambda \ll 1$ limit, with a noticeable decay in performance as λ approaches the critical value of 2. For $\lambda > 2$, localization forces the fidelity to the limit of 0.5, with the resonant case ($E_0 = 0$) demonstrating superior robustness in the transition region.

Furthermore, the maximum simulation time $T_{\max} = 6 \times 10^5\ \hbar/\mathrm{J}$ is consistent with typical experimental estimates for quantum information transfer protocols [15]. In particular, according to perturbation theory, the characteristic transfer time in weak-coupling regimes is expected to scale as $1/g^2$. Therefore, our choice of $T_{\max}$ provides a sufficiently long window to capture the complete evolution of the excitation and accurately determine the maximum fidelity, even in the intermediate regimes where the effective Thouless velocity is significantly reduced.

3. Results and discussion

The transport efficiency in the source–channel–receiver setup is intrinsically governed by the spatial and spectral properties of the underlying Aubry-André chain. By analyzing the interplay between localization measures and dynamical observables, we characterize the metal–insulator transition and its implications for quantum communication.

The localization transition is further elucidated via the Green's function formalism in Fig. 1. The LDOS ratio ρ_{geo}/ρ_{arith} acts as a useful statistical indicator, remaining near unity in the metallic phase and vanishing for $\lambda > 2$, signaling the onset of log-normal spectral distributions typical of the localized regime. A striking feature is observed in the neighbor propagator $\langle|G_{i,i+1}|\rangle$, which exhibits a pronounced peak at the critical point $\lambda = 2$. This pronounced peak originates from the closing of spectral gaps and the critical resonance of states at the transition, where the hybridization of modes is maximized before exponential confinement takes over. In the metallic phase ($\lambda < 2$), the probability amplitude is delocalized over the entire chain, causing a dilution that suppresses the local propagator. In contrast, the onset of localization forces a spatial confinement of the wavefunction, which concentrates the probability density and consequently enhances the short-range propagator elements. Finally, the spatial decay parameter D remains zero in the delocalized phase and grows linearly for $\lambda > 2$. This confirms that for $\lambda > \lambda_c$, the wavefunctions are exponentially confined, whereas for $\lambda < 2$, the vanishing of D supports the extended nature of the states, even as their transport velocity collapses due to spectral fragmentation.

Fig. 2 illustrates the maximum average fidelity $\bar{F}_{\max}$ for an Aubry-André chain of $N = 100$ sites as a function of the quasiperiodic potential strength λ (with $g = 0.05$). Although Fibonacci system sizes are conventionally used to minimize commensurability effects in bulk studies, we emphasize that practical implementations of quantum state transfer typically utilize relatively short chains due to current experimental constraints. To ensure the reliability of our findings and discard finite-size artifacts, we performed additional simulations across multiple system sizes, specifically $N = 89$,144, and 233. For each size, we evaluated both the exact golden ratio $\beta = (\sqrt{5} - 1)/2$ and its corresponding rational approximations ($\beta = 89/144$ or $144/233$). Aside from small quantitative deviations in specific regions, the results exhibit good qualitative agreement with the $N = 100$ case. Specifically, as the system size increases up to two or three times our base length, we observe a slight natural decay in the overall baseline fidelity. Nevertheless, within the near-ballistic regime ($\lambda \lesssim 1$), the transfer efficiency remains remarkably robust and close to the maximum ideal value. This minor reduction in fidelity with increasing N is physically expected: as the wave packet traverses a longer distance, it undergoes natural spatial dispersion and accumulates minor phase fluctuations over the extended transit time, preventing a perfectly rigid wave-packet reconstruction at the receiver. This confirms that the observed transport phenomena, particularly the sharp fidelity degradation in the delocalized phase, are robust physical features of the model and not numerical artifacts stemming from finite-size constraints or the specific rational approximation of β. While the theoretical metal–insulator transition for the standard Aubry-André model occurs at $\lambda_c = 2$, the transport efficiency reveals a more complex behavior. For $\lambda \ll 1$, the system remains deep in the extended regime, enabling fidelities close to unity. However, as λ increases beyond 1.0, even though the bulk states are still formally delocalized, F_{max} begins to degrade significantly, falling well below 1. This suggests that the increased quasiperiodic potential leads to the scattering of the wave packet or induces effective off-resonance conditions prior to the absolute localization threshold. Interestingly, the resonant case ($E_0 = 0$) maintains higher fidelity over a wider range, showing greater robustness. Finally, for $\lambda > 2$, the system enters the fully localized regime. In this phase, wave packet propagation is strongly suppressed due to exponential localization, causing the fidelity to saturate exactly at 0.5. We note that this value naturally emerges from the mathematical definition of $\bar{F}(t)$: when the source and receiver are effectively decoupled and the transition amplitude vanishes ($f(t) \to 0$), the formulation inherently reduces to this limit, reflecting a complete lack of communication between the boundary channels.

A crucial observation in this study is the significant degradation of the maximum average fidelity $\bar{F}_{\max}$ in the interval $1 \lesssim \lambda < 2$. Despite the system remaining formally in the delocalized phase, the strengthening quasiperiodic potential introduces substantial phase fluctuations and reduces the Thouless velocity of the mediating modes. This dynamic transport crossover is associated with a strong suppression of the Thouless velocity $\langle v_T \rangle$, caused by progressive spectral fragmentation and band flattening as the system approaches the localization transition. In this slow-transport extended regime, although the eigenstates remain spatially extended, the resulting spectral compression, characterized by significantly flattened energy bands, implies that wave packets experience a drastic reduction in propagation speed alongside increased spatial dispersion. Consequently, the quantum excitation reaches the receiver significantly delayed and spatially broadened, leading to destructive interference that hinders constructive reconstruction. This dynamical bottleneck causes $\bar{F}_{\max}$ to drop noticeably below ideal values long before the Anderson localization threshold at $\lambda_c = 2$ is reached. To quantify this transport collapse, we calculate the Thouless energy $\mathcal{E}_T$, which provides a measure of the effective transport speed. Physically, an extended state with a high velocity is highly sensitive to a change in boundary conditions, whereas slow modes in flattened bands become insensitive to the boundaries long before they become exponentially localized. It is important to emphasize that the periodic and anti-periodic boundary conditions used to compute $\mathcal{E}_T$ are applied strictly to the isolated channel Hamiltonian H_{ch}. This procedure allows us to probe the intrinsic sensitivity of bulk states to phase shifts at the boundaries, independently of the external source and receiver couplings employed in the transport setup. The diagonalization was performed using a shift-invert spectral transformation to accurately target eigenstates near $E_0 = 0$. A small regulator $\sigma = 10^{-10}$ was introduced to avoid numerical singularities in the tridiagonal matrix inversion. Statistical convergence was ensured by averaging over $M = 1000$ random phase realizations.

The spatial nature of the eigenstates of the isolated Aubry-André channel is first characterized in Fig. 3(a) by analyzing the scaling of the participation ratio (PR) with the system size N. To rigorously rule out finite-size artifacts, these scaling calculations were performed using very large Fibonacci numbers, ranging from $N = 987$ up to approximately 122,000. The results confirm that, throughout the delocalized phase ($\lambda < 2$), the eigenstates remain spatially extended, as evidenced by the extensive scaling of the PR ($PR \propto N$). This confirms that the channel supports modes spanning the entire lattice, theoretically providing a continuous path for quantum information. However, a complete understanding of the transport efficiency requires the dynamical analysis shown in Fig. 3(b). The numerical results, derived from the scaling of the Thouless energy $\mathcal{E}_T$, successfully capture the substantial suppression of the Thouless velocity $\langle v_T \rangle$ as the quasiperiodic potential strength λ increases toward the critical threshold $\lambda_c = 2$. Notably, these Thouless velocity curves were calculated for multiple large Fibonacci sizes, specifically $N = 1597, 2584$, and 4181. The fact that the transport collapse remains qualitatively identical across these scales further guarantees that this is a genuine macroscopic feature of the crossover regime. As the quasiperiodic modulation strengthens, the resulting fragmentation and flattening of the energy bands drastically reduce the spectral sensitivity to boundary conditions, which translates dynamically into a severe reduction in the propagation speed of wave packets. The juxtaposition of these spatial and dynamical metrics confirms that the observed degradation in quantum state transfer fidelity in the interval $1 \lesssim \lambda < 2$ is not a consequence of spatial localization. Instead, it is fundamentally driven by the strongly suppressed transport speed of the mediating modes near the band center. In this

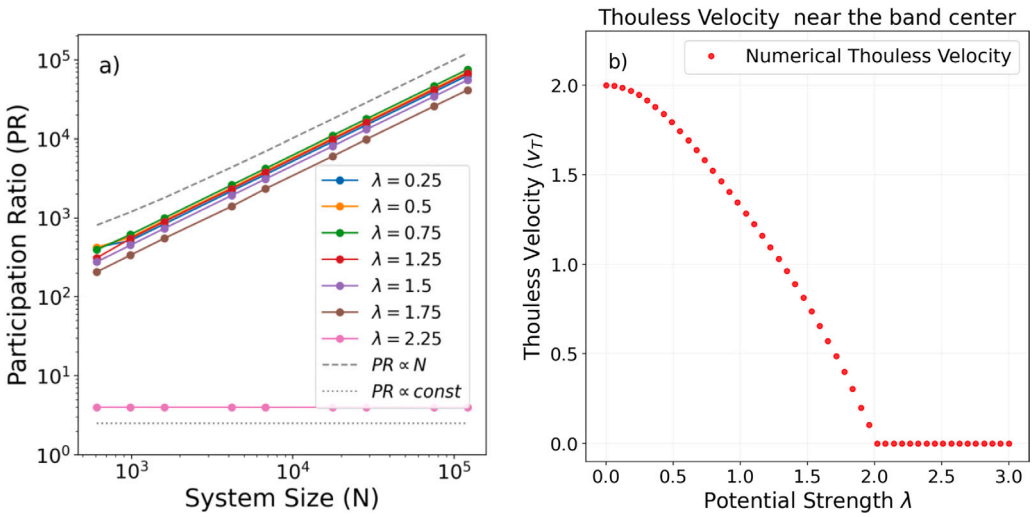

Fig. 3. Spatial and dynamical characterization of the Aubry-André channel near the band center ($E \approx 0$). (a) Scaling of the Participation Ratio (PR) with system size N for representative potential strengths $\lambda = 0.25, 0.5, 0.75, 1.25, 1.5, 1.75$ (extended phase) and $\lambda = 2.25$ (localized phase). To rule out finite-size effects, calculations were performed using Fibonacci numbers ranging from $N = 987$ up to $N \approx 1.22 \times 10^5$. The power-law behavior $PR \propto N^{D_2}$ with $D_2 \approx 1$ confirms that states remain spatially extended throughout the metallic phase ($\lambda < 2$), whereas the collapse to $PR \sim \mathcal{O}(1)$ signals the onset of exponential localization. (b) Effective Thouless velocity $\langle v_T \rangle$ derived from the Thouless energy $\mathcal{E}_T$ as a function of λ. The calculations were verified across multiple large Fibonacci system sizes ($N = 1597, 2584$, and 4181), yielding qualitatively identical behavior. The numerical results capture the smooth collapse of the transport speed as the system approaches the critical threshold $\lambda_c = 2$. Together, these results demonstrate that the degradation in quantum state transfer fidelity observed for $1 < \lambda < 2$ is not driven by spatial confinement, but is fundamentally caused by the strongly suppressed velocity of the mediating modes due to spectral fragmentation.

slow-transport extended regime, although the states remain extended without any exponential confinement, they become increasingly "slow" and highly dispersive. Consequently, the quantum excitation reaches the receiver site with significant delay and spatial broadening, hindering the coherent constructive interference required for high-fidelity reconstruction. This mechanism causes the transfer fidelity to drop noticeably long before the genuine Anderson localization threshold is reached. Finally, to ensure complete generality, the studies presented in Fig. 3 were performed using both the exact irrational golden ratio $\beta = (\sqrt{5}-1)/2$ and its corresponding rational approximations $\beta = F_{n-1}/F_n$. Moreover, we verified the consistency of these scaling trends by testing arbitrary system sizes that do not belong to the Fibonacci sequence (e.g., $N = 1000, 2000, 4000, \ldots, 120{,}000$). The results remained virtually indistinguishable. This remarkably weak dependence on whether N is a Fibonacci number, as well as on the specific nature of β, is primarily mediated by the ensemble average over the random phases ϕ, which smooths out local commensurability effects and reveals the robust underlying bulk physics.

Complementing the previous analysis of F_{max} versus λ, Fig. 4 focuses on the influence of the terminal-chain coupling strength g on the transfer efficiency. The calculations were performed for the resonant case ($E_0 = 0$) with g evaluated in the range $0.01 \leq g \leq 0.225$. Rather than a strictly monotonic mathematical function, it is observed that within this evaluated window, the fidelity exhibits a systematic, pronounced decrease as g increases for all values of λ in the extended regime. This behavior indicates that although a stronger coupling might naively suggest a faster signal injection, it ultimately results in an impedance mismatch at the boundaries, inducing backscattering that severely hinders the coherent transfer of the quantum state. Particularly for $\lambda < 1$, where the system is nearly ballistic, the fidelity reaches values close to unity only for weak couplings ($g \ll 0.1$). As g increases, the degradation of F_{max} becomes severe, suggesting that the injection rate becomes incompatible with the internal propagation dynamics of the quasiperiodic chain. Furthermore, the clear separation between the curves for different λ values reinforces that quasi-disorder and coupling strength act as competing mechanisms for fidelity loss. However, it is important to emphasize that optimizing this process involves a practical trade-off: while a weak coupling minimizes destructive boundary scattering, an

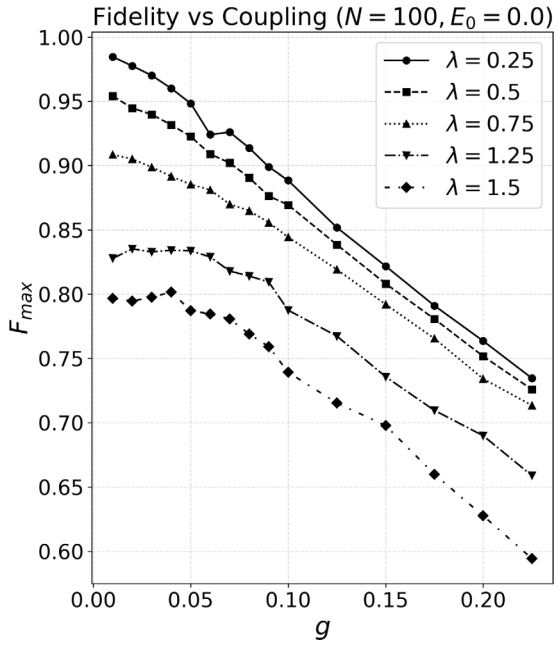

Fig. 4. Maximum fidelity (F_{max}) as a function of the coupling g evaluated in the range $[0.01, 0.225]$. For $\lambda = 0.5$, the fidelity remains near unity for $g < 0.05$ but drops by approximately 20% as g increases to 0.2, illustrating the impedance mismatch effect.

excessively small g would dramatically increase the required transfer time. Thus, the optimal window for high-precision operations lies in a weak-coupling regime that carefully balances impedance matching with timely signal injection, rather than an arbitrarily small coupling.

Fig. 5 depicts the dependence of the spectral correlation C on the potential strength λ for different injection energies E_0. This quantity measures the effective overlap between the source and receiver sites mediated by the eigenstates of the Aubry-André channel. In the ballistic

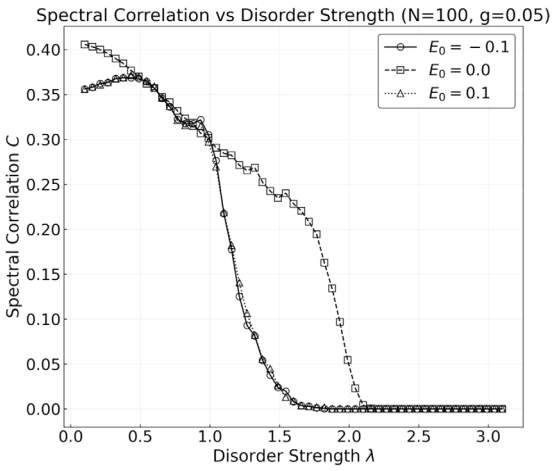

Fig. 5. Spectral correlation C as a function of the quasi-disorder strength λ for a chain of length $N = 100$ and boundary coupling $g = 0.05$. The data compares the resonant injection at the band center ($E_0 = 0$, dashed line with squares) against slightly detuned injection energies ($E_0 = \pm 0.1$, solid and dotted lines). The resonant case exhibits superior robustness, maintaining high spectral overlap close to the critical point $\lambda_c = 2$, whereas off-resonant modes experience a sharp suppression of correlations around $\lambda \approx 1$.

limit ($\lambda \to 0$), all considered energies exhibit significant correlation values, indicating a high potential for quantum state transfer. However, a distinct behavior emerges as the quasiperiodic modulation increases. For the resonant case ($E_0 = 0$), the spectral correlation remains robust throughout the metallic phase, sustaining a high plateau until the vicinity of the localization transition at $\lambda_c = 2$. At this critical point, C drops sharply to zero, consistent with the localization of the eigenstates which decouples the boundaries. In contrast, for the scenarios ($E_0 = \pm 0.1$), the correlation begins to degrade significantly earlier, exhibiting a rapid decay around $\lambda \approx 1$.. This early suppression suggests that even small detunings from the band center render the spectral connectivity highly sensitive to spectral fragmentation, effectively breaking the transfer channel well before the global metal–insulator transition occurs. Consequently, operation at the precise band center ($E_0 = 0$) is identified as a critical requirement for maximizing the resilience of quantum transport against quasiperiodic disorder. These findings corroborate the fidelity studies discussed previously, offering a static perspective on the transport efficiency. The early suppression of C for ($E_0 \neq 0$) closely mirrors the degradation of transfer quality in the delocalized phase, while the robust spectral connectivity at $E_0 = 0$ explains the resilience of the resonant protocol. This correspondence establishes spectral correlation as a reliable predictor of dynamical performance in aperiodic channels. While the condition $E_0 = 0$ aligns the source and receiver with the band center, the local potential at the boundary sites $n = 1$ and $n = N$ varies with the random phase ϕ. Consequently, the "resonant" injection described here should be understood in a statistical sense: after averaging over ϕ, the energy mismatch is effectively compensated, allowing the band-center modes to dominate the transport dynamics.

4. Conclusion

In this work, we have investigated the relationship between the localization landscape of the Aubry-André model and its efficacy as a quantum interconnect. Our results highlight that relying solely on the conventional dichotomy between extended and localized phases is insufficient to predict the efficiency of quantum state transfer (QST) in finite chains. While the system remains spatially delocalized for $\lambda < 2$, we observed a dynamic transport crossover in the slow-transport extended regime ($1 \lesssim \lambda < 2$) where the transport quality severely degrades. As evidenced by the extensive scaling of the Participation Ratio, this degradation is not driven by spatial confinement. Rather, it originates from the fragmentation and flattening of the energy bands, which leads to a strongly suppressed Thouless velocity and significant dispersive broadening of the propagating wave packet.

Furthermore, our analysis of the static spectral correlation C provides valuable insights into the robustness of these channels against energy detuning. We demonstrated that, upon disorder-phase averaging, the band-center injection ($E_0 = 0$) is highly resilient, maintaining substantial spectral overlap between the source and receiver up to the vicinity of the critical point $\lambda_c = 2$. In contrast, slightly detuned states ($E_0 \neq 0$) experience a rapid suppression of boundary correlations at quasiperiodic modulation strengths ($\lambda \approx 1$) well below the metal–insulator transition. Additionally, we found that high-fidelity transfer favors weak boundary coupling ($g \ll J$) to minimize destructive scattering, though we note that extreme weak coupling must be carefully balanced against proper impedance matching to ensure timely signal injection. Consequently, optimal QST in finite quasiperiodic chains is largely restricted to the near-ballistic limit ($\lambda \lesssim 1$) under precise resonant conditions.

In summary, we emphasize that successful quantum state transfer in aperiodic potentials depends on a delicate balance that transcends the traditional localization length criterion. Our findings reveal that the severe suppression of the average Thouless velocity, driven by spectral band flattening, can hinder information propagation nearly as effectively as exponential Anderson localization. For future quantum engineering applications, this implies that ensuring a high Participation Ratio is a necessary but not sufficient condition; one must also explicitly optimize for the Thouless velocity within the transmission window. This dynamical constraint constitutes a key practical design consideration for the deployment of aperiodic chains as reliable quantum data buses.

CRediT authorship contribution statement

D.G.P. da Silva: Data curation, Conceptualization. **I.F.F. dos Santos:** Data curation, Conceptualization. **B.G.S. Souza:** Data curation, Conceptualization. **W.F. Magalhães:** Data curation. **G.M.A. Almeida:** Data curation, Conceptualization. **F.A.B.F. de Moura:** Writing – review & editing, Writing – original draft, Visualization, Validation, Supervision, Software, Resources, Project administration, Methodology, Investigation, Funding acquisition, Formal analysis, Data curation, Conceptualization.

Declaration of competing interest

The authors declare that they have no known competing financial interests or personal relationships that could have appeared to influence the work reported in this paper.

Acknowledgments

The authors acknowledge the financial and institutional support from CNPq, CAPES, and FAPEAL.

Data availability

Data will be made available on request.

References

[1] S. Bose, Quantum communication through an unmodulated spin chain, Phys. Rev. Lett. 91 (20) (2003) 207901.

[2] M. Christandl, N. Datta, A. Ekert, A.J. Landahl, Perfect state transfer in quantum spin networks, Phys. Rev. Lett. 92 (18) (2004) 187902.

[3] A. Kay, Perfect, efficient, state transfer and its application as a constructive tool, Int. J. Quantum Inf. 8 (04) (2010) 641–676.

[4] D. Burgarth, S. Bose, Perfect quantum state transfer with randomly coupled quantum chains, New J. Phys. 7 (1) (2005) 135.

[5] M. Christandl, N. Datta, T.C. Dorlas, A. Ekert, A. Kay, A.J. Landahl, Perfect transfer of arbitrary states in quantum spin networks, Phys. Rev. A 71 (3) (2005) 032312.

[6] C. Albanese, M. Christandl, N. Datta, A. Ekert, Mirror inversion of quantum states in linear registers, Phys. Rev. Lett. 93 (23) (2004) 230502.

[7] M.-H. Yung, Quantum speed limit for perfect state transfer in one dimension, Phys. Rev. A 74 (3) (2006) 030303.

[8] S. Aubry, G. André, Analyticity breaking and Anderson localization in incommensurate lattices, Ann. Isr. Phys. Soc. 3 (133) (1980) 18.

[9] Y. Lahini, R. Pugatch, F. Pozzi, M. Sorel, R. Morandotti, N. Davidson, Y. Silberberg, Observation of a localization transition in quasiperiodic photonic lattices, Phys. Rev. Lett. 103 (1) (2009) 013901.

[10] Y.E. Kraus, Y. Kafri, R. Pugatch, Four-dimensional quantum Hall effect in a two-dimensional quasicrystal, Phys. Rev. Lett. 111 (2013) 226401.

[11] J. Hermisson, U. Grimm, M. Baake, Aperiodic and correlated disorder in XY chains: exact results, J. Phys. A: Math. Gen. 30 (21) (1997) 7315.

[12] G. Roati, C. D'Errico, L. Fallani, M. Fattori, C. Fort, M. Zaccanti, G. Modugno, M. Modugno, M. Inguscio, Anderson localization of a non-interacting Bose–Einstein condensate, Nature 453 (7197) (2008) 895–898.

[13] J. Billy, V. Josse, Z. Zuo, A. Bernard, B. Hambrecht, P. Lugan, D. Clément, L. Sanchez-Palencia, P. Bouyer, A. Aspect, Direct observation of Anderson localization of matter waves in a controlled disorder, Nature 453 (7197) (2008) 891–894.

[14] G. Modugno, Exponential localization in one-dimensional quasi-periodic optical lattices, New J. Phys. 11 (3) (2009) 033023.

[15] D. Messias, C.V.C. Mendes, G.M.A. Almeida, M.L. Lyra, F.A.B.F. de Moura, Rabi-like quantum communication in an aperiodic spin-1/2 chain, J. Magn. Magn. Mater. 505 (2020) 166730, http://dx.doi.org/10.1016/j.jmmm.2020.166730.

[16] J.M. Luck, Cantor spectra and scaling of gap widths in deterministic aperiodic systems, Phys. Rev. B 39 (9) (1989) 5834.

[17] X. Deng, S. Ray, S. Sinha, G.V. Shlyapnikov, L. Santos, One-dimensional quasicrystals with power-law hopping, Phys. Rev. Lett. 123 (2019) 025301.

[18] S. Ganeshan, K. Sun, S. Das Sarma, Topological zero-energy modes in gapless commensurate Aubry–André–Harper models, Phys. Rev. Lett. 110 (2013) 180403.

[19] S. Sutradhar, A. Rajak, B.K. Chakrabarti, Controlled quantum state transfer in XX spin chains at the quantum speed limit, Phys. Rev. E 99 (2019) 032115.

[20] T.J. Apollaro, L. Banchi, A. Cuccoli, R. Vaia, P. Verrucchi, Many-qubit quantum state transfer via spin chains, Phys. Rev. A 85 (5) (2012) 052319.

[21] S. Paganelli, S. Lorenzo, T.J. Apollaro, F. Plastina, G.L. Giorgi, Routing quantum information in spin chains, Phys. Rev. A 87 (2013) 062309.

[22] A. Barbosa, J. Lima, I. Bezerra, M. Lyra, Electronic transport in disordered graphene superlattices with scale-free correlated barrier spacements, Phys. E 133 (2021) 114210, http://dx.doi.org/10.1016/j.physe.2020.114210.

[23] J. Chakrian, M. Lyra, J. Lima, Metallic insulator phase transitions in the power-law modulated Harper model, Phys. E 158 (2024) 115887.

[24] A. MacKinnon, B. Kramer, Localization: theory and experiment, Rep. Progr. Phys. 56 (12) (1993) 1469–1566, http://dx.doi.org/10.1088/0034-4885/56/12/001.

[25] H. Fried, D. Barragan-Yani, F. Libisch, et al., A machine learning approach to predict tight-binding parameters for point defects via the projected density of states, NPJ Comput. Mater. 11 (2025) 176, http://dx.doi.org/10.1038/s41524-025-01634-1, URL https://www.nature.com/articles/s41524-025-01634-1.

[26] M. Sonner, M. Serbyn, Z. Papić, D.A. Abanin, Thouless energy across the many-body localization transition in Floquet systems, Phys. Rev. B 104 (2021) L081112, http://dx.doi.org/10.1103/PhysRevB.104.L081112, URL https://link.aps.org/doi/10.1103/PhysRevB.104.L081112.